

Stable computation of entanglement entropy for two-dimensional interacting fermion systemsGaopei Pan^{1,2,*}, Yuan Da Liao^{3,4,†}, Weilun Jiang^{1,2}, Jonathan D’Emidio⁵, Yang Qi^{3,4,6}, and Zi Yang Meng^{7,‡}¹*Beijing National Laboratory for Condensed Matter Physics and Institute of Physics, Chinese Academy of Sciences, Beijing 100190, China*²*School of Physical Sciences, University of Chinese Academy of Sciences, Beijing 100049, China*³*State Key Laboratory of Surface Physics, Fudan University, Shanghai 200438, China*⁴*Center for Field Theory and Particle Physics, Department of Physics, Fudan University, Shanghai 200433, China*⁵*Donostia International Physics Center, P. Manuel de Lardizabal 4, 20018 Donostia-San Sebastián, Spain*⁶*Collaborative Innovation Center of Advanced Microstructures, Nanjing 210093, China*⁷*Department of Physics and HKU-UCAS Joint Institute of Theoretical and Computational Physics, The University of Hong Kong, Pokfulam Road, Hong Kong SAR, China*

(Received 2 April 2023; revised 23 May 2023; accepted 14 August 2023; published 28 August 2023)

There is no doubt that the information hidden in entanglement entropy (EE), for example, the n th order Rényi EE, i.e., $S_n^A = \frac{1}{1-n} \ln \text{Tr}(\rho_A^n)$, where $\rho_A = \text{Tr}_{\bar{A}}\rho$ is the reduced density matrix, can be used to infer the organizing principle of two-dimensional (2D) interacting fermion systems, ranging from spontaneous symmetry-breaking phases and quantum critical points to topologically ordered states. It is far from clear, however, whether EE can be obtained with the precision required to observe these fundamental features—usually in the form of universal finite-sized scaling behavior. Even for the prototypical 2D interacting fermion model—the Hubbard model—to all existing numerical algorithms, the computation of EE has not been successful with reliable data from which the universal scaling regime can be accessed. Here, we explain the reason for these unsuccessful attempts of EE computations in quantum Monte Carlo simulations in the past decades and, more importantly, show how to overcome the conceptual and computational barrier with the incremental algorithm, such that the stable computation of EE in 2D interacting fermion systems can be achieved and universal scaling information can be extracted. Relevance toward experimental 2D interacting fermion systems is discussed.

DOI: [10.1103/PhysRevB.108.L081123](https://doi.org/10.1103/PhysRevB.108.L081123)**I. INTRODUCTION**

Entanglement witnesses can reveal the fundamental organizing principle of quantum many-body systems [1–21]. One such witness is entanglement entropy (EE), i.e., the n th order Rényi EE $S_n^A = \frac{1}{1-n} \ln \text{Tr}(\rho_A^n)$, where $\rho_A = \text{Tr}_{\bar{A}}\rho$ is the reduced density matrix of a many-body Hamiltonian [4–8,12,22–36]. EE is an important quantity for the investigations of two-dimensional (2D) and higher-dimensional interacting fermion systems, as it can reveal the fundamental conformal field theory (CFT) data for the fermionic quantum critical points [1,4–6], the nature of the low-energy collective modes [12,22–24,30–32,35,36], and the topological information [7,8], which are usually difficult to compute otherwise. Therefore, the ability to compute the scaling behavior of EE for 2D interacting fermion systems holds the key to understanding properties of non-Fermi-liquid and strange metal states in high-temperature superconductivity, phases in quantum moiré materials, fermion quantum criticalities, topological ordered states, etc. However, as we will explain below, the stable computation of EE for 2D interacting fermion

systems has not been successful despite many attempts over the past decades.

The EE of free fermion systems can be derived via the Widom-Sobolev formula [14,32,33,37–40] and results in the $L \ln(L)$ scaling of a free Fermi surface in 2D [14,32–36]. The universal log coefficient beyond the area law scaling for free Dirac fermions has also been obtained [6,14,15,41,42]. The computation of EE for interacting fermion lattice models in 2D has not been successful, with notable exceptions including topological EE computed from fractional quantum Hall ground states [43,44].

Since the computation of EE in 2D interacting fermion lattice models requires access to a many-body wave function or partition function [4–8], the auxiliary-field determinant quantum Monte Carlo (DQMC) method becomes a good tool to possibly obtain EE in the exponentially large Hilbert space [22–24,26,30,31,45–49]. In the past decades, significant algorithmic advances in the computation of Rényi EE have been made. This was spearheaded by Grover [22], who used the free fermion decomposition of the reduced density matrix to identify an estimator based on independent auxiliary-field configurations. Despite its elegance, early implementations of this approach revealed severe statistical errors at strong coupling and not-even-large subsystem sizes [23,24]. This motivated translating the highly successful replica approach from path-integral spin systems [50] into the auxiliary-field fermion language [45–47], which however

* gppan@iphy.ac.cn† ydliao@fudan.edu.cn‡ zymeng@hku.hk

proved cumbersome since it required introducing a replicated environment for the entangling subsystem and using an imaginary time-dependent Hamiltonian, thus substantially increasing the computation burden [the computational complexity of DQMC scales as $O(\beta N^3)$, with $\beta = \frac{1}{T}$ the inverse temperature and $N = L^d$ for d spatial dimension systems with linear size L]. Furthermore, it suffered from subtle stability issues regarding the computation of Green's functions. All attempts thus far in computing Rényi EE for interacting fermions in 2D have not achieved the precision required to extract, in the simplest square lattice Hubbard model, an area law plus universal log due to Goldstone modes [51].

On the other hand, since the quantum Monte Carlo (QMC) computational complexity in spin/boson systems scales as $O(\beta N)$, the EE of 2D Heisenberg models [50,52–55] and other related systems [12,56] has had much success, although the data quality is always a serious issue for extracting the expected universal scaling coefficients. This problem is completely solved by the introduction of the *incremental* algorithm [25,27–29]. The algorithm converts the computation of the Rényi EE into the parallel execution of the Jarzynski equality [57] of the free energy difference between partition functions on replicated manifolds, making the precise determination of EE scaling on various 2D quantum spin models possible with exquisite data quality. By using the algorithm, controlled results with the expected CFT information can then be obtained, including in the Néel phase of the antiferromagnetic Heisenberg model, at the (2+1)D O(3) quantum critical point, the deconfined quantum critical point, and inside the Z_2 topological ordered kagome quantum spin liquid [27–29], to name a few.

It is in the process of developing the *incremental* algorithm into DQMC for the entanglement computation in interacting fermion systems [30] that we understand the reason why the previous *direct* implementation of EE computation [22–24,26,45–47] does not work—not because of the heavy computation added to the already expensive DQMC by adding replicas but because the direct computation does not use the correct sampling weight to construct a proper Markov chain Monte Carlo simulation. The incremental algorithm [30,31], on the other hand, features two key improvements:

(1) designing the effective Monte Carlo importance sampling weight for EE computations and

(2) conditioning the exponentially small partition function ratio into a parallel execution of values with scales of unity;

and consequently offers the correct scheme that can be utilized to extract the EE with reliable data quality and controllable polynomial computation complexity. Here, we use the prototypical example of 2D interacting fermion lattice models—the square lattice Hubbard model—to fully explain the simple but fundamental breakthrough of the incremental over the previous direct computation of EE. The algorithm opens the avenue for the stable EE computation for 2D fermion quantum matter and can be used to extract the universal information for the quantum critical metal and non-Fermi liquid [14,58–67], the fermion deconfined quantum critical point [15,31,68,69], the correlated flat-band Moiré materials [70–75], kagome metals [76–78], and the entanglement spectra and Hamiltonian [9,11,13,16,23,46,79], which cannot be accessed with other methods.

II. MODEL AND METHOD

We study the second Rényi EE for the square lattice Hubbard model at half-filling, with the Hamiltonian $H = -t \sum_{\langle i,j \rangle} (c_{i,\sigma}^\dagger c_{j,\sigma} + \text{H.c.}) + \frac{U}{2} \sum_i (n_{i,\uparrow} + n_{i,\downarrow} - 1)^2$, where $c_{i,\sigma}^\dagger$ and $c_{i,\sigma}$ denote the creation and annihilation operators with spin $\sigma = \uparrow, \downarrow$ on site i , $\langle i, j \rangle$ represents the nearest-neighbor hopping, $n_{i,\sigma} = c_{i,\sigma}^\dagger c_{i,\sigma}$ is the particle number operator for spin σ , and U/t tunes the on site interaction strength, with $t = 1$ the energy unit.

We utilize the projector DQMC method to compute the Rényi EE. As described in the Supplemental Material (SM) [80] and the literature [58–60,70–72,81,82], it carries out a Hubbard-Stratonovich transformation to introduce an auxiliary field $\{s\}$ to decouple the quartic fermion interaction and compute ground-state observables as $\langle O \rangle = \frac{\sum_{\{s\}} W^s(O)^s}{\sum_{\{s\}} W^s}$, where W^s is the unnormalized weight of configuration s proportional to a determinant whose elements depend on s [80]. To calculate the Rényi EE of interacting fermions in DQMC, Grover [22] introduced a direct formula based on the free fermion decomposition of the reduced density matrix ρ_A (with entangling region A) using two independent auxiliary field replicas, such that the second Rényi EE S_2^A is given by

$$\exp(-S_2^A) = \frac{Z(1)}{Z(0)} := \frac{\sum_{\{s_1, s_2\}} \mathbf{W}^{s_1, s_2} \det g_A^{s_1, s_2}}{\sum_{\{s_1, s_2\}} \mathbf{W}^{s_1, s_2}}, \quad (1)$$

where $\mathbf{W}^{s_1, s_2} = W^{s_1} W^{s_2}$, and $g_A^{s_1, s_2} = G_A^{s_1} G_A^{s_2} + (\mathbb{I} - G_A^{s_1})(\mathbb{I} - G_A^{s_2})$ is the Grover [22] matrix connecting the Green's functions G^{s_1} and G^{s_2} of the two replicas on A . Here, $Z(1)$ stands for the partition function with the fully connected entangling region between the two replicas and $Z(0)$ the partition function of two independent replicas; we use $\lambda \in [0, 1]$ to parametrize the evolution from $Z(\lambda = 0)$ to $Z(\lambda = 1)$.

Based on Eq. (1), one can compute S_2^A as in conventional DQMC simulations with the configurational weights \mathbf{W}^{s_1, s_2} , and this is indeed what has been implemented in previous attempts [22–24]. However, it was noticed that the obtained EE suffered greatly from a numerical instability issue with poor data quality that cannot be used to extract the universal scaling behavior:

$$S_2^A(L) = aL \ln L + bL + s \ln L + c, \quad (2)$$

where the coefficients a stem from the 2D Fermi surface and can be derived at the noninteracting limit [14,32–37] (see Eq. (S7) and Fig. S1 in the SM [80]), b governs the area law scaling, and s is the universal corner contribution at critical points [5,6,12] or is proportional to the number of Goldstone modes in symmetry-broken phases [51]. For example, for the 2D Hubbard model at $U = 8$, $s = \frac{N_G}{2} = 1$, where $N_G = 2$ is the number of Goldstone modes for a Néel state (see Fig. 2), a result that has eluded implementations using the direct approach of Grover [22].

What has been seen, however, is that, for slightly larger system sizes ($L \geq 8$) and slightly stronger interactions ($U \geq 4$), the distribution of the Grover determinants became very broad with spikes (rare events). We find, if one insists on direct computation of EE with Eq. (1), it is these rare events that actually make great contributions to the expectation value of EE, but since they occur less often with respect to L and U ,

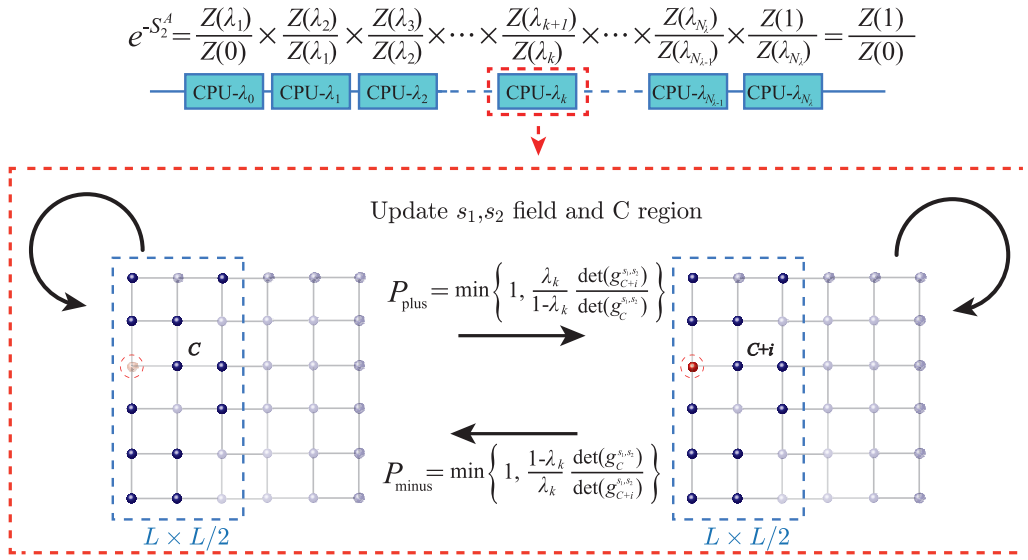


FIG. 1. The incremental computation of entanglement entropy (EE). The entanglement region A is denoted as the blue dashed box. According to Eq. (3), we split the computation into the parallel execution of many ratios, where each ratio is bounded with a scale of unity and the sites inside A for each parallel piece are not fixed but change stochastically. The adding and removing sites (denoted as the red dot and dashed circle) in A are carried out with probabilities P_{plus} and P_{minus} . The quantum Monte Carlo (QMC) updates of the auxiliary field for each parallel piece are carried out independently. When we update the s_1, s_2 field, the sites in A and in the environment are fixed, as denoted by the circular arrows.

one will certainly run into a problem with increased L and U . This means the direct computation of EE in Eq. (1) follows the incorrect distribution \mathbf{W}^{s_1, s_2} and consequently does not average according to the important sampling of a Markov chain Monte Carlo process.

To address this issue, i.e., to sample properly in the replicated configurational space of EE computation, the incremental algorithm for fermions was recently developed in Ref. [30] and further applied in Ref. [31]. As sketched in Fig. 1, the incremental algorithm has improved the direct computation in two main points:

First, it introduces a new auxiliary sampling configuration, namely, the subset C of the entanglement region A , which instead of calculating $\exp(-S_2^A)$ directly converts the computation of $\exp(-S_2^A)$ into a parallel execution of incremental ratios as

$$\begin{aligned} \exp(-S_2^A) &= \frac{Z(1)}{Z(0)} \\ &:= \frac{Z(\lambda_1)}{Z(0)} \frac{Z(\lambda_2)}{Z(\lambda_1)} \dots \frac{Z(\lambda_{k+1})}{Z(\lambda_k)} \dots \frac{Z(1)}{Z(\lambda_{N_k})}, \end{aligned} \quad (3)$$

where $Z(\lambda) = \sum_{C \subseteq A} \lambda^{N_C} (1-\lambda)^{N_A - N_C} Z_C$ [27,30] with $\lambda \in [0, 1]$, N_C (N_A) is the number of sites in region C (A), and $Z_C = \sum_{\{s_1\}, \{s_2\}} \mathbf{W}^{s_1, s_2} \det g_C^{s_1, s_2}$. Here, N_λ is the number of λ_k . Further, $\frac{Z(\lambda_{k+1})}{Z(\lambda_k)}$ is computed as

$$\frac{Z(\lambda_{k+1})}{Z(\lambda_k)} = \frac{\sum_{\{s_1, s_2, C \subseteq A\}} \mathbf{W}_C^{s_1, s_2}(\lambda_k) O_C(\lambda_k, \lambda_{k+1})}{\sum_{\{s_1, s_2, C \subseteq A\}} \mathbf{W}_C^{s_1, s_2}(\lambda_k)}, \quad (4)$$

where the observable for the EE is $O_C(\lambda_k, \lambda_{k+1}) = \binom{\lambda_{k+1}}{\lambda_k}^{N_C} \left(\frac{1-\lambda_{k+1}}{1-\lambda_k}\right)^{N_A - N_C}$, and the sampling weight of the EE computation is

$$\mathbf{W}_C^{s_1, s_2}(\lambda_k) = \lambda_k^{N_C} (1-\lambda_k)^{N_A - N_C} \mathbf{W}^{s_1, s_2} \det g_C^{s_1, s_2}. \quad (5)$$

We note the weight ratio $\frac{\mathbf{W}_C^{s_1, s_2}(\lambda_k)}{\mathbf{W}_C^{s_1, s_2}(\lambda_k)} = \frac{W^{s_1} \det g_C^{s_1, s_2}}{W^{s_1} \det g_C^{s_1, s_2}}$ of incremental sampling in Eq. (4) is explicitly different from that of direct sampling $\frac{W^{s_1, s_2}}{W^{s_1}} = \frac{W^{s_1}}{W^{s_1}}$ in Eq. (1), in that it contains the contribution from the determinant of the Grover matrix. In addition, the incremental method updates the configurations C stochastically with probabilities P_{plus} and P_{minus} for adding or moving one site from region C , as shown in Fig. 1. When sampling

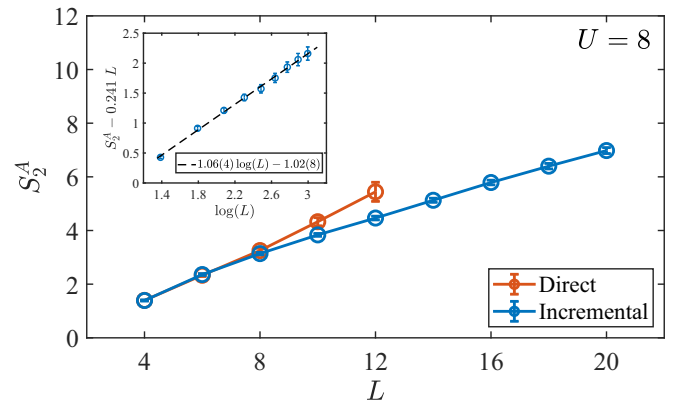


FIG. 2. Entanglement entropy (EE) of the square lattice Hubbard model at $U = 8$. The entanglement region A is of size $L \times L/2$. The red and blue lines are from the direct and incremental methods, respectively. The deviation of the direct computation for $L \geq 8$ is obvious. The inset shows the incremental data of $S_2^A - 0.241L$ vs $\log(L)$, with the slope (denoted as the black dashed line) representing the universal log coefficient $s = \frac{N_G}{2} = 1$ in Eq. (2); our fitting results of $s = 1.06(4)$ are fully consistent with the expected behavior of a Néel antiferromagnetic Mott insulator with $N_G = 2$. It is important to note that the error bars of direct data (red dots) are unestimated, as the mean values have not converged, as shown in Fig. 4.

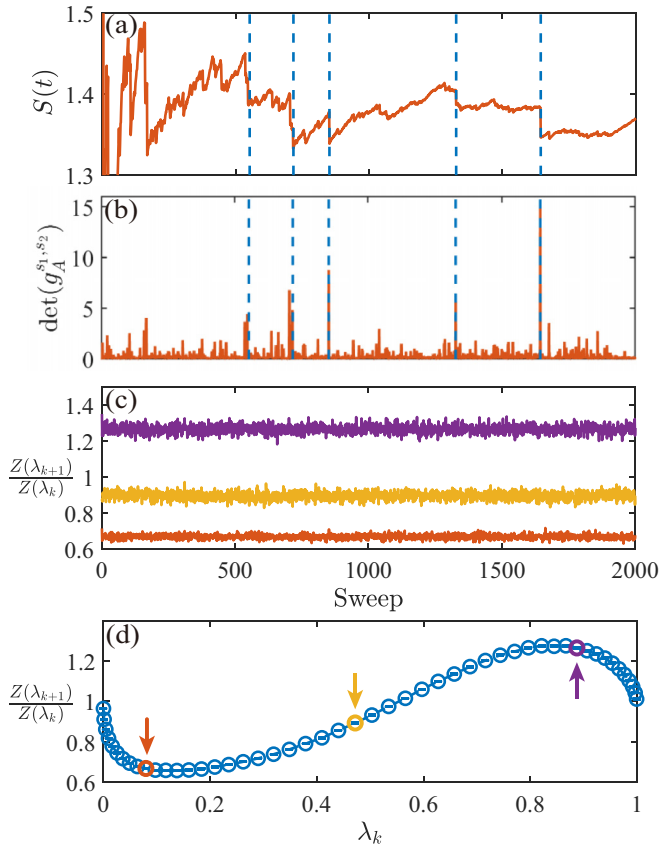


FIG. 3. Difference between direct and incremental measurements. (a) and (b) show the time series of $\det(g_A^{S_1, S_2})$ and $S(t)$ from a single Markov chain using a direct method with $U = 8$, $L = 4$. Both observables are clearly not normally distributed, and rare events in the form of the sudden drop in (a) and spikes in (b), denoted by blue dotted lines, are clearly seen. (c) and (d) $\frac{Z(\lambda_{k+1})}{Z(\lambda_k)}$ for $U = 8$, $L = 10$ by the incremental method with $\lambda \in [0, 1]$. The number of λ_k , N_λ is 50, and each piece has the value of scale unity. The three arrows in (d) point out the position of three different λ_k values whose time series are shown in (c). The observables are now normally distributed.

according to Eq. (5), there will be no spikes in the observable $O_C(\lambda_k, \lambda_{k+1})$, provided λ_k and λ_{k+1} are close enough such that their histograms of N_C overlap. The ensemble average can then be properly carried out.

Second, we find each piece of the ratio $\frac{Z(\lambda_{k+1})}{Z(\lambda_k)}$ in Eq. (3) can be computed independently, which means massive parallelization of high-performance computation (denoted in Fig. 1) can greatly reduce the computation time. Although $\exp(-S_2^A)$ is eventually an exponentially small quantity, each piece in the product of Eq. (3) has a well-behaved bound of the scale of unity; since the independent computation of $\frac{Z(\lambda_{k+1})}{Z(\lambda_k)}$ is very well behaved, their product gives rise to controlled EE with the same polynomial complexity as DQMC. The increments $\frac{Z(\lambda_{k+1})}{Z(\lambda_k)}$ of $O(1)$ and their histograms in the noninteracting cases are shown in the SM [80] (see also Ref. [83] therein).

III. RESULTS IN 2D HUBBARD MODEL

We have carried out EE computation for the square lattice Hubbard model with $L = 4, 8, 10, 12, 16$, and 20. Most of

our data are obtained at $U = 8$, where the system is in the antiferromagnetic Mott insulator state. The $U = 0$ limit is discussed in the SM [80], where the computed $aL \ln L$ with the coefficient $a = \frac{1}{2}$ in Eq. (2) was obtained in full agreement with the analytic expectation from the Widom-Sobolev formula [14,32,37–40].

The results of EE at $U = 8$ are shown in Fig. 2. Here, the entanglement region is half of the lattice: $L/2 \times L$. One clearly sees that, when the system size L is small, the results of the two methods coincide, but when the size gradually increases, the mean value of the direct method starts to deviate from the expected behavior of the incremental one.

Moreover, since the half-filled square lattice Hubbard model is always in an antiferromagnetic Mott insulating phase ($U > 0$), the S_2^A of the system with spontaneous broken $SU(2)$ continuous symmetry should have a form in Eq. (2) with $a = 0$, b finite, and the universal log-coefficient $s = \frac{N_G}{2} = 1$, where $N_G = 2$ is the number of the Goldstone modes [12,51]. As shown in the inset of Fig. 2, the log coefficient after extracting the area law term is 1.06(4), very consistent with

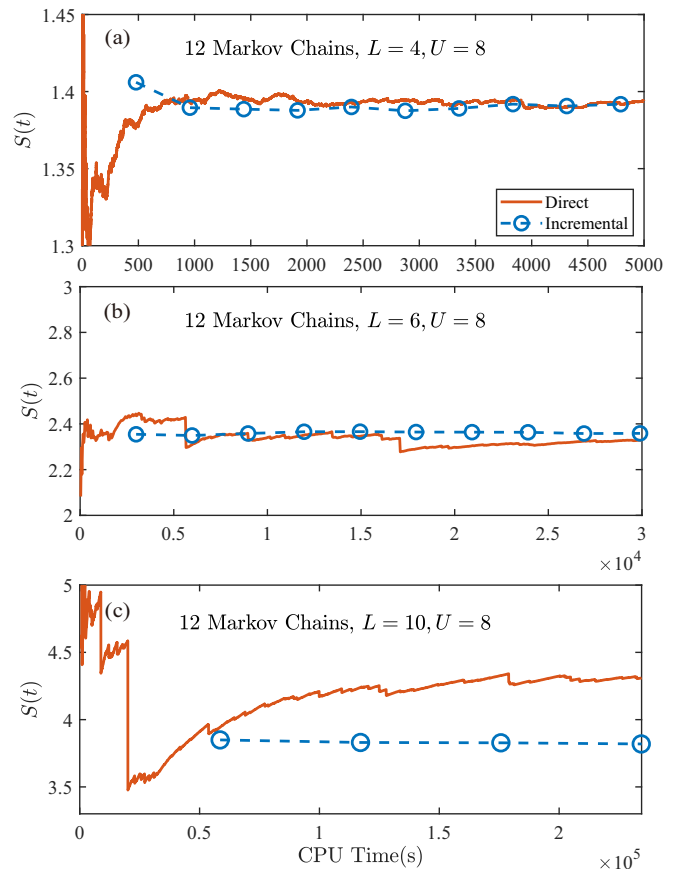


FIG. 4. Convergence comparison between the direct and incremental methods. (a) For $L = 4$, $U = 8$, the direct method (red line) can slowly converge to an exact value, while the incremental method (blue dots) converges fast. (b) For $L = 6$, $U = 8$, the direct method converges within a reasonable central processing unit (CPU) time but with big fluctuations; the incremental method converges fast. (c) For $L = 10$, $U = 8$, the direct method cannot converge within a reasonable CPU time; the incremental method converges fast.

the theoretical expected value 1. The results of the direct computation will not be able to perform such an analysis.

To reveal the difference between the two methods, we record the time series of EE computation along the Markov chain, $S(t) = -\ln[\frac{1}{t} \sum_{i=1}^t \exp(-S_2^A(i))]$, where $S(t)$ represents the expectation value of observable S_2^A after the first t DQMC sweeps. As shown in Fig. 3(b), for the direct method, S_2^A does not follow normal distribution, and whenever a peak is sampled, there is an obvious drop in the mean value of EE calculated, as shown in Fig. 3(a). The $S(t)$ is affected by these rare events, which renders the direct computation with very poor performance. As L and U increase, a very long Markov chain is needed to obtain accurate values, as shown in Fig. 3(b) and the red lines in Fig. 4. In fact, from Fig. 4(c), one sees for $L = 10$ and $U = 8$ that the direct $S(t)$ has not converged. The incremental EE has no problem. For each parallel piece, the range of the observable is controlled as we have considered the determinant of the Grover matrix in the weight during sampling in Eq. (5). In Fig. 3(d), the range of the partition function ratios is given, with $L = 10$, $U = 8$, and $\lambda_k = [\sin \frac{(0.002+50(k-1))\pi}{2}]^2$. And the sampling distributions of three colored points are shown in Fig. 3(c). The incremental method with its fast convergence and parallel computation clearly outperforms direct computation.

IV. DISCUSSION

By utilizing the square lattice Hubbard model, we reveal the fundamental difference between the direct and incremental computation of EE in that the two major improvements: (i) designing the effective Monte Carlo sampling weight and

(ii) conditioning the exponential factor of partition function ratios into parallel execution of values with scale of unity; bestow the incremental method access to the entanglement scaling behavior of 2D interacting fermion models. Our approach establishes the paradigm of EE computation for 2D highly entangled fermion quantum matter and has the potential to offer universal experimentally measurable quantities to guide experiments in quantum critical metal and non-Fermi-liquid [14,58–67], the fermion deconfined quantum critical point [15,31,68,69], the correlated flat-band Moiré materials [70–75] and kagome metals [76–78], and the entanglement spectra and Hamiltonian in 2D interacting fermion systems [9,11,13,16,23,46,79].

ACKNOWLEDGMENTS

We thank Jiarui Zhao and Zheng Yan for collaborations on the incremental algorithm for spin/boson systems [28,29] and inspiring discussions on the related topic. We thank Fakher Assaad for bringing our attention to the instability issue of EE computation over the years. G.P.P., W.L.J., and Z.Y.M. acknowledge support from the Research Grants Council (RGC) of the Hong Kong Special Administrative Region (SAR) of China (Projects No. 17301420, No. 17301721, No. AoE/P-701/20, No. 17309822, and No. HKU C7037-22G), and the ANR/RGC Joint Research Scheme sponsored by the RGC of Hong Kong SAR of China and the French National Research Agency (Project No. A_HKU703/22). Y.D.L. acknowledges support from the National Natural Science Foundation of China (Grant No. 12247114) and the China Postdoctoral Science Foundation (Grants No. 2021M700857 and No. 2021TQ0076).

-
- [1] J. L. Cardy and I. Peschel, *Nucl. Phys. B* **300**, 377 (1988).
 - [2] M. Srednicki, *Phys. Rev. Lett.* **71**, 666 (1993).
 - [3] C. Holzhey, F. Larsen, and F. Wilczek, *Nucl. Phys. B* **424**, 443 (1994).
 - [4] P. Calabrese and J. Cardy, *J. Stat. Mech.: Theory Exp.* (2004) P06002.
 - [5] E. Fradkin and J. E. Moore, *Phys. Rev. Lett.* **97**, 050404 (2006).
 - [6] H. Casini and M. Huerta, *Nucl. Phys. B* **764**, 183 (2007).
 - [7] A. Kitaev and J. Preskill, *Phys. Rev. Lett.* **96**, 110404 (2006).
 - [8] M. Levin and X.-G. Wen, *Phys. Rev. Lett.* **96**, 110405 (2006).
 - [9] H. Li and F. D. M. Haldane, *Phys. Rev. Lett.* **101**, 010504 (2008).
 - [10] H. F. Song, S. Rachel, C. Flindt, I. Klich, N. Laflorencie, and K. Le Hur, *Phys. Rev. B* **85**, 035409 (2012).
 - [11] Z. Yan and Z. Y. Meng, *Nat. Commun.* **14**, 2360 (2023).
 - [12] N. Laflorencie, *Phys. Rep.* **646**, 1 (2016).
 - [13] A. Chandran, V. Khemani, and S. L. Sondhi, *Phys. Rev. Lett.* **113**, 060501 (2014).
 - [14] W. Jiang, B.-B. Chen, Z. H. Liu, J. Rong, F. F. Assaad, M. Cheng, K. Sun, and Z. Y. Meng, *arXiv:2209.07103* (2022).
 - [15] Z. H. Liu, W. Jiang, B.-B. Chen, J. Rong, M. Cheng, K. Sun, Z. Y. Meng, and F. F. Assaad, *Phys. Rev. Lett.* **130**, 266501 (2023).
 - [16] D. Poilblanc, *Phys. Rev. Lett.* **105**, 077202 (2010).
 - [17] Y.-C. Wang, M. Cheng, and Z. Y. Meng, *Phys. Rev. B* **104**, L081109 (2021).
 - [18] B.-B. Chen, H.-H. Tu, Z. Y. Meng, and M. Cheng, *Phys. Rev. B* **106**, 094415 (2022).
 - [19] Y.-C. Wang, N. Ma, M. Cheng, and Z. Y. Meng, *SciPost Phys.* **13**, 123 (2022).
 - [20] M. Song, J. Zhao, L. Janssen, M. M. Scherer, and Z. Y. Meng, *arXiv:2307.02547* (2023).
 - [21] M. Song, J. Zhao, Y. Qi, J. Rong, and Z. Y. Meng, *arXiv:2306.05465* (2023).
 - [22] T. Grover, *Phys. Rev. Lett.* **111**, 130402 (2013).
 - [23] F. F. Assaad, T. C. Lang, and F. Parisen Toldin, *Phys. Rev. B* **89**, 125121 (2014).
 - [24] C.-C. Chang, R. R. P. Singh, and R. T. Scalettar, *Phys. Rev. B* **90**, 155113 (2014).
 - [25] V. Alba, *Phys. Rev. E* **95**, 062132 (2017).
 - [26] F. Parisen Toldin and F. F. Assaad, *Phys. Rev. Lett.* **121**, 200602 (2018).
 - [27] J. D’Emidio, *Phys. Rev. Lett.* **124**, 110602 (2020).
 - [28] J. Zhao, Y.-C. Wang, Z. Yan, M. Cheng, and Z. Y. Meng, *Phys. Rev. Lett.* **128**, 010601 (2022).
 - [29] J. Zhao, B.-B. Chen, Y.-C. Wang, Z. Yan, M. Cheng, and Z. Y. Meng, *npj Quantum Mater.* **7**, 69 (2022).

- [30] J. d’Emidio, R. Orus, N. Laflorencie, and F. de Juan, *arXiv:2211.04334* (2022).
- [31] Y. Da Liao, G. Pan, W. Jiang, Y. Qi, and Z. Y. Meng, *arXiv:2302.11742* (2023).
- [32] B. Swingle, *Phys. Rev. Lett.* **105**, 050502 (2010).
- [33] R. Hellings, H. Leschke, and W. Spitzer, *Int. Math. Res. Not.* **2011**, 1451 (2010).
- [34] M. Cramer, J. Eisert, and M. B. Plenio, *Phys. Rev. Lett.* **98**, 220603 (2007).
- [35] T. Barthel, M.-C. Chung, and U. Schollwöck, *Phys. Rev. A* **74**, 022329 (2006).
- [36] R. V. Mishmash and O. I. Motrunich, *Phys. Rev. B* **94**, 081110(R) (2016).
- [37] D. Gioev and I. Klich, *Phys. Rev. Lett.* **96**, 100503 (2006).
- [38] H. Leschke, A. V. Sobolev, and W. Spitzer, *Phys. Rev. Lett.* **112**, 160403 (2014).
- [39] A. V. Sobolev, *J. Funct. Anal.* **266**, 5886 (2014).
- [40] A. V. Sobolev, *Integr. Equ. Oper. Theory* **81**, 435 (2015).
- [41] S. Sahoo, E. M. Stoudenmire, J.-M. Stéphan, T. Devakul, R. R. P. Singh, and R. G. Melko, *Phys. Rev. B* **93**, 085120 (2016).
- [42] J. Helmes, L. E. Hayward Sierens, A. Chandran, W. Witczak-Krempa, and R. G. Melko, *Phys. Rev. B* **94**, 125142 (2016).
- [43] M. P. Zaletel, R. S. K. Mong, and F. Pollmann, *Phys. Rev. Lett.* **110**, 236801 (2013).
- [44] W. Zhu, S. S. Gong, F. D. M. Haldane, and D. N. Sheng, *Phys. Rev. Lett.* **115**, 126805 (2015).
- [45] P. Broecker and S. Trebst, *J. Stat. Mech.: Theory Exp.* (2014) P08015.
- [46] F. F. Assaad, *Phys. Rev. B* **91**, 125146 (2015).
- [47] P. Broecker and S. Trebst, *Phys. Rev. E* **94**, 063306 (2016).
- [48] Y. D. Liao, *arXiv:2307.10602* (2023).
- [49] Z. H. Liu, Y. D. Liao, G. Pan, W. Jiang, C.-M. Jian, Y.-Z. You, F. F. Assaad, Z. Y. Meng, and C. Xu, *arXiv:2308.07380* (2023)
- [50] M. B. Hastings, I. González, A. B. Kallin, and R. G. Melko, *Phys. Rev. Lett.* **104**, 157201 (2010).
- [51] M. A. Metlitski and T. Grover, *arXiv:1112.5166* (2011).
- [52] A. B. Kallin, M. B. Hastings, R. G. Melko, and R. R. P. Singh, *Phys. Rev. B* **84**, 165134 (2011).
- [53] S. Humeniuk and T. Roscilde, *Phys. Rev. B* **86**, 235116 (2012).
- [54] J. Helmes and S. Wessel, *Phys. Rev. B* **89**, 245120 (2014).
- [55] B. Kulchitskyy, C. M. Herdman, S. Inglis, and R. G. Melko, *Phys. Rev. B* **92**, 115146 (2015).
- [56] S. V. Isakov, M. B. Hastings, and R. G. Melko, *Nat. Phys.* **7**, 772 (2011).
- [57] C. Jarzynski, *Phys. Rev. Lett.* **78**, 2690 (1997).
- [58] Y. D. Liao, X. Y. Xu, Z. Y. Meng, and Y. Qi, *Phys. Rev. B* **106**, 075111 (2022).
- [59] Y. D. Liao, X. Y. Xu, Z. Y. Meng, and Y. Qi, *Phys. Rev. B* **106**, 115149 (2022).
- [60] Y. D. Liao, X. Y. Xu, Z. Y. Meng, and Y. Qi, *Phys. Rev. B* **106**, 155159 (2022).
- [61] X. Y. Xu, Z. H. Liu, G. Pan, Y. Qi, K. Sun, and Z. Y. Meng, *J. Phys.: Condens. Matter* **31**, 463001 (2019).
- [62] Z. H. Liu, G. Pan, X. Y. Xu, K. Sun, and Z. Y. Meng, *Proc. Natl. Acad. Sci. USA* **116**, 16760 (2019).
- [63] G. Pan, W. Jiang, and Z. Y. Meng, *Chin. Phys. B* **31**, 127101 (2022).
- [64] X. Y. Xu, K. Sun, Y. Schattner, E. Berg, and Z. Y. Meng, *Phys. Rev. X* **7**, 031058 (2017).
- [65] A. A. Patel, H. Guo, I. Esterlis, and S. Sachdev, *Science* **381**, 790 (2023).
- [66] I. Esterlis, H. Guo, A. A. Patel, and S. Sachdev, *Phys. Rev. B* **103**, 235129 (2021).
- [67] P. Lunts, M. S. Albergo, and M. Lindsey, *Nat. Commun.* **14**, 2547 (2023).
- [68] M. Christos, Z.-X. Luo, H. Shackleton, Y.-H. Zhang, M. S. Scheurer, and S. Sachdev, *Proc. Natl. Acad. Sci. USA* **120**, e2302701120 (2023).
- [69] Y. Liu, Z. Wang, T. Sato, M. Hohenadler, C. Wang, W. Guo, and F. F. Assaad, *Nat. Commun.* **10**, 2658 (2019).
- [70] Y. Da Liao, Z. Y. Meng, and X. Y. Xu, *Phys. Rev. Lett.* **123**, 157601 (2019).
- [71] Y. D. Liao, J. Kang, C. N. Breið, X. Y. Xu, H.-Q. Wu, B. M. Andersen, R. M. Fernandes, and Z. Y. Meng, *Phys. Rev. X* **11**, 011014 (2021).
- [72] Y.-D. Liao, X.-Y. Xu, Z.-Y. Meng, and J. Kang, *Chin. Phys. B* **30**, 017305 (2021).
- [73] G. Pan, X. Zhang, H. Lu, H. Li, B.-B. Chen, K. Sun, and Z. Y. Meng, *Phys. Rev. Lett.* **130**, 016401 (2023).
- [74] X. Zhang, G. Pan, B.-B. Chen, H. Li, K. Sun, and Z. Y. Meng, *Phys. Rev. B* **107**, L241105 (2023).
- [75] C. Huang, X. Zhang, G. Pan, H. Li, K. Sun, X. Dai, and Z. Y. Meng, *arXiv:2304.14064* (2023).
- [76] J.-X. Yin, B. Lian, and M. Z. Hasan, *Nature (London)* **612**, 647 (2022).
- [77] M. Kang, L. Ye, S. Fang, J.-S. You, A. Levitan, M. Han, J. I. Facio, C. Jozwiak, A. Bostwick, E. Rotenberg *et al.*, *Nat. Mater.* **19**, 163 (2020).
- [78] S. Sankar, R. Liu, X.-J. Gao, Q.-F. Li, C. Chen, C.-P. Zhang, J. Zheng, Y.-H. Lin, K. Qian, R.-P. Yu *et al.*, *arXiv:2303.03274* (2023).
- [79] M. Song, J. Zhao, Z. Yan, and Z. Y. Meng, *Phys. Rev. B* **108**, 075114 (2023).
- [80] See Supplemental Material at <http://link.aps.org/supplemental/10.1103/PhysRevB.108.L081123> where we discuss in detail the projector DQMC algorithm and the implementation of the incremental algorithm for EE computation therein. We also provide the exact results of EE at the noninteracting limits as well as the convergence and histogram of the partition function ratio and Grover determinant for the interacting system considered in the main text.
- [81] F. Assaad and H. Evertz, in *Computational Many-Particle Physics*, edited by H. Fehske, R. Schneider, and A. Weiße (Springer, Berlin, Heidelberg, 2008), Vol. 739, pp. 277–356.
- [82] X. Y. Xu, Y. Qi, L. Zhang, F. F. Assaad, C. Xu, and Z. Y. Meng, *Phys. Rev. X* **9**, 021022 (2019).
- [83] P. Calabrese, M. Mintchev, and E. Vicari, *Europhys. Lett.* **98**, 20003 (2012).